Beamspace Transform for UCA: Error Analysis and Bias Reduction

Fabio Belloni, *Student Member, IEEE*, and Visa Koivunen, *Senior Member, IEEE*

***Abstract*—In this paper, we analyze the error caused by the beamspace transform (BT) when it is applied to uniform circular array (UCA) configuration. Several algorithms for direction of arrival (DoA) estimation exploit this modal transform because it allows using computationally efficient techniques such as polynomial rooting and dealing with coherent sources. The BT is based on the phase-mode excitation principle. The performance of such DoA estimators is degraded if the array has a small number of elements. We introduce a modified beamspace transform (MBT) that performs mapping from element-space to beamspace domain taking into account the error caused by the transform. Justification of the difference in the statistical performances of MUSIC and root-MUSIC algorithms for UCA is also given. Moreover, we show that there is a significant difference in the performance of the UCA root-MUSIC technique depending on whether an even or odd number of elements is used. We derive an expression approximating the bias in the DoA estimates that is caused by the beamspace transform. Some design guidelines are provided for choosing the key UCA configuration parameters such as number of sensors, array radius, and interelement spacing in order to reduce the error. Finally, we propose a novel technique for bias removal. It allows practically bias-free DoA estimation.**

***Index Terms*—Array calibration, beamspace and modified beamspace transform, bias reduction, direction of arrival (DoA) estimation, error analysis, uniform circular array (UCA), uniform linear array (ULA).**

I. Introduction

CIRCULAR arrays are of interest in a variety of applications, e.g., in multiantenna communication transceivers, navigation, and electronic intelligence. Moreover, uniform circular arrays (UCAs) have uniform performance regardless of the angle of arrival and can estimate both azimuth and elevation angles simultaneously. In order to come up with computationally efficient high-resolution direction of arrival (DoA) estimators for circular array, the so-called beamspace transform (BT) may be applied. It rebuilds desired Vandermonde structure for the steering vectors. Consequently, methods like root-MUSIC, ESPRIT, and special versions of MUSIC may be applied to find DoAs [2], [4]. Notice that in this paper, we consider the case of azimuthal estimation at a fixed elevation angle.

Manuscript received October 7, 2004; revised September 19, 2005. The associate editor coordinating the review of this manuscript and approving it for publication was Dr. Vikram Krishnamurthy. This work was supported by grants from the Finnish Defence Forces Research Centre and Academy of Finland, SMARAD Center of Excellence program.

The authors are with SMARAD Center of Excellence, Signal Processing Laboratory, Department of Electrical Engineering, Helsinki University of Technology, FIN-02015 HUT, Finland (e-mail: fbelloni@wooster.hut.fi; visa@wooster.hut.fi).

Digital Object Identifier 10.1109/TSP.2006.877664

The BT works properly only under certain conditions on the array configuration that may be difficult to satisfy in some applications. For example, when a UCA with a small number of sensors (from six to ten elements) is used, a residual error due to the beamspace transform introduces a bias in the DoA estimates. Obviously, the Cramér–Rao lower bound (CRB) cannot be achieved then.

In this paper, we present a qualitative and quantitative analysis of the residual error in order to analyze the behavior of the algorithms and improve their performance. We derive a modified version of the BT that shows that the error can be interpreted as element misplacement. An expression for the residual error is found and a first-order approximation of the bias in the DoA estimates is introduced. Moreover, some rules of thumb for choosing the key parameters in a UCA configuration are given. In practice, the configuration parameters of a UCA may be selected to provide a good tradeoff among different design goals.

In the case of uniform linear array (ULA), well-known noise subspace algorithms such as MUSIC and root-MUSIC have similar asymptotical performance [15]. In this paper, we show that this is not the case when those techniques are applied to UCA configuration. They have asymptotically equal performances only when a UCA with a suitable configuration is used. Otherwise the algorithms, in particular the root-MUSIC method, suffer from bias caused by the BT. We will also show that there is a significant difference in performance whether even or odd number of sensors are used in a UCA.

In this paper, we introduce an iterative technique for removing the bias introduced by the BT. Expressions for two correction terms that eliminate the bias are derived. Consequently, the estimates become practically bias-free, as will be demonstrated in the simulations.

This paper is organized as follows. First, the UCA system model is presented. In Section III, the phase-mode excitation principle is described. In Section IV, we define the BT and an expression for the residual error. A modified beamspace transform (MBT) is introduced. In Section V, effects of the residual error on the DoA estimates are shown. A first-order approximation of the bias in the DoA estimates is found. In Section VI, simulation results illustrating the dependence of the residual term on the UCA configuration parameters are shown. The differences in performance between the MUSIC and root-MUSIC techniques for UCA are explained. In Section VII, a novel technique for bias removal is presented. Section VIII concludes this paper.

II. Signal Model

Let us have a UCA of N sensors. There are P emitters lying on the array plane $(P < N)$. The transmitted narrow-band sig-

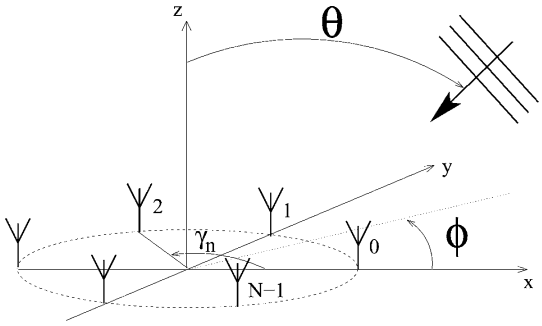

Fig. 1. UCA with N elements. The wavefield impinges to the array from a direction denoted by θ (elevation) and ϕ (azimuth). The array lies on the xy plane.

nals are impinging the array from directions $\phi_1, \phi_2, \ldots, \phi_P$ (ϕ is the azimuth angle). Furthermore, we assume that K snapshots are observed by the array. The $N \times K$ element-space array output matrix $\mathbf{X}$ is modelled as

$$\mathbf{X} = \mathbf{AS} + \mathbf{N} \tag{1}$$

where $\mathbf{A}$ is the $N \times P$ element-space array steering vector matrix, $\mathbf{S}$ is the $P \times K$ source matrix, and $\mathbf{N}$ is the $N \times K$ noise matrix. The noise is modelled as a stationary, second-order ergodic, zero-mean spatially and temporally white circular complex Gaussian process. The element-space steering vector matrix of a UCA may be written as $\mathbf{A} = [\mathbf{a}_1(\zeta, \phi), \ldots, \mathbf{a}_P(\zeta, \phi)]$, where each column is of the form

$$\mathbf{a}_p(\boldsymbol{\vartheta}) = \left[e^{j\zeta\cos(\phi_p - \gamma_0)}, e^{j\zeta\cos(\phi_p - \gamma_1)}, \ldots, e^{j\zeta\cos(\phi_p - \gamma_{(N-1)})}\right]^T \tag{2}$$

for $p = 1, 2, \ldots, P$. Here $\boldsymbol{\vartheta} = (\zeta, \phi)$ and $\zeta = \kappa r \sin\theta, r$ is the radius, $\kappa = (\omega/c)$ is the wavenumber, c is the wave propagation speed, $\omega = 2\pi f$ is the angular frequency, and $\gamma_n = (2\pi n)/(N)$ $(n = 0, \ldots, N-1)$ is the sensor location. The elevation angle θ is measured down from the z axis. In this paper, it is assumed to be fixed at 90°, i.e., the sensor plane. The azimuth angle ϕ is measured counterclockwise from the x axis; see Fig. 1.

III. Phase-Mode Excitation Principle

In this section, the phase-mode excitation principle [1], [2] is described. The BT considered in this paper is based on this principle. Hence, a brief overview is given first.

We proceed by first considering a continuous circular array. This array model cannot be realized but is the ideal configuration for applying the principle and leads to an error-free scenario. Then we move to the discrete circular array (e.g., UCA) that represents a more practical configuration. Already at this stage we can see why the residual error occurs.

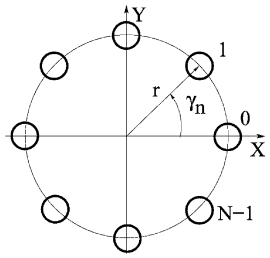

Fig. 2. UCA with $N = 8$ sensors; r as the radius, and $\gamma_n = (2\pi n)/(N)$ $(n = 0, \ldots, N-1)$ as the angular position of a sensor.

A. Continuous Circular Aperture

In the case of continuous circular aperture, any excitation function is periodic in γ with a period of 2π and can hence be expressed in terms of Fourier series [1], [2], [19]. A generic excitation function $w(\gamma)$ may be defined using the inverse Fourier series $w(\gamma) = \sum_{m=-\infty}^{\infty} c_m e^{jm\gamma}$, where the mth phase mode $w_m(\gamma) = e^{jm\gamma}$ represents a spatial harmonic of the array excitation, c_m is the corresponding Fourier series coefficient, and γ represents the angular location of a point, which runs continuously on the circular aperture.

By integrating the spatial harmonic of the array excitation $w_m(\gamma)$ over the continuous circular array, we can compute the normalized far-field pattern $f_m^c(\boldsymbol{\vartheta})$ resulting from exciting the aperture with the mth mode as [1], [2]

$$f_m^c(\boldsymbol{\vartheta}) = \frac{1}{2\pi}\int_0^{2\pi} w_m(\gamma) e^{j\zeta\cos(\phi-\gamma)}\,\mathrm{d}\gamma. \tag{3}$$

Equation (3) can be also expressed by using Bessel function properties as

$$f_m^c(\boldsymbol{\vartheta}) = j^m J_m(\zeta) e^{jm\phi} \tag{4}$$

where $J_m(\zeta)$ is the Bessel function of the first kind of order m; see Appendix II for more details.

The far-field pattern $f_m^c(\boldsymbol{\vartheta})$ has the same azimuthal variation $e^{jm\phi}$ as the excitation function itself. This property allows an attractive direction pattern to be synthesized using phase-mode excitation [1]. Instead, the amplitude and elevation dependence of the far-field pattern is through the Bessel function. For this reason, only a finite number of modes can be excited by a given circular aperture. The rule for computing the highest order mode M is to consider the smallest integer that is close or equal to κr. In this way the excitation modes are $m \in [-M, M]$. For more details, see [2] and [19].

B. Discrete Circular Aperture

A UCA is a discrete version of the continuous circular array where a finite number of sensors is uniformly placed along a circle; see Fig. 2.

TABLE I
RESIDUAL TERM OF THE EXCITATION MODE $m = -2, -1, 0, 1, 2$ AS A FUNCTION OF THE PARAMETER q. THE TERMS CORRESPONDING TO $q = 2, 3$ ARE VERY SMALL WITH RESPECT TO THE DOMINANT ONE, FOR $q = 1$

m	$q = 1$	$q = 2$	$q = 3$
-2	$3.4974e-3$	$1.4712e-10$	$5.3643e-20$
-1	$6.3276e-4$	$1.1874e-11$	$2.8291e-21$
0	$3.3232e-5$	$1.7015e-12$	$1.4261e-22$
1	$6.3276e-4$	$1.1874e-11$	$2.8291e-21$
2	$3.4974e-3$	$1.4712e-10$	$5.3643e-20$

For UCAs, the normalized beamforming weight vector that excites the array with phase mode $m \in [-M, M]$ is [1], [2]

$$\mathbf{w}_m^H = \frac{1}{N}[e^{jm\gamma_0}, e^{jm\gamma_1}, \ldots, e^{jm\gamma_{N-1}}] \tag{5}$$

where m is the excitation order, N is the number of sensors, γ_n is the angular location of the nth sensor, and $(\cdot)^H$ stands for conjugate transpose. Consequently, the array beampattern may be formed as

$$f_m^s(\boldsymbol{\vartheta}) = \mathbf{w}_m^H \mathbf{a}(\boldsymbol{\vartheta}) = \frac{1}{N}\sum_{n=0}^{N-1} e^{jm\gamma_n} e^{j\zeta\cos(\phi-\gamma_n)} \tag{6}$$

where $\mathbf{a}(\boldsymbol{\vartheta})$ is the UCA element-space steering vector in (2). For mode order $|m| \leq M$, (6) can be rewritten as [1], [2]

$$\begin{aligned} f_m^s(\boldsymbol{\vartheta}) &= j^m J_m(\zeta) e^{jm\phi} + \sum_{q=1}^{\infty}(j^g J_g(\zeta) e^{-jg\phi} + j^h J_h(\zeta) e^{jh\phi}) \\ &= j^m J_m(\zeta) e^{jm\phi} + \varepsilon_m \end{aligned} \tag{7}$$

where the variable ε_m represents the entire sum term above and the indexes g and h are defined as $g = Nq - m$ and $h = Nq + m$.

Equation (7) is composed of two terms. The first term is named the *principal term* and is identical to the far-field pattern of the continuous array. The latter *residual term* ε_m arises from the sampling of the continuous aperture by N sensors. This component, known as higher order distortion mode, has to be minimized in order to get close to ideal (continuous) case performance [2]. Here the subscript m refers to the residual term associated with the mth excitation mode.

In Table I, the numerical values of the magnitude of the first three components of the residual term (for $q = 1, 2, 3$) for different excitation mode orders m are given. The values are computed by considering an UCA with $N = 8$ sensors, radius $r = (\lambda/2.6)$, and source operating at $f = 1.8$ GHz and impinging on the array from $(\phi, \theta) = (55°, 90°)$. Observe that even though the residual term ε_m is given as a sum of an infinite number of terms, only the first one (for $q = 1$) is significant. By expanding the sum we can see that the numerical values of the terms rapidly decrease as the index q increases because q is proportional to the order of the Bessel functions. This kind of behavior is independent of the DoA of the sources, and the first component of the residual term always remains dominant.

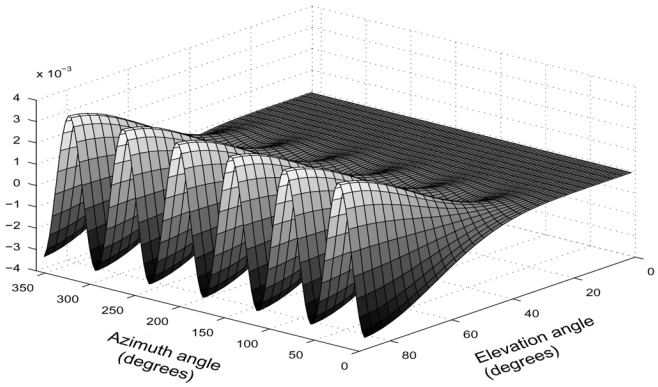

Fig. 3. Residual term as function of both azimuth ϕ and elevation θ angles. UCA settings: $N = 8, r = (\lambda/2.6)$ and $f = 1.8$ GHz.

Looking at the residual term, we realize that it depends on both the azimuth and elevation angles. For this reason, the systematic error in the DoA estimates is not constant but depends on the actual angle of arrival. In Fig. 3, the angular dependence of the residual term is shown as a function of ϕ and θ. Here, the residual term decreases as the elevation angle changes from 90° to 0° while it appears to behave like a sinusoid as a function of the azimuth angle. In the plot, we have depicted the real part of the Mth excitation mode.

By analyzing (7) we find that the principal term remains dominant by setting $N > 2|m|$. Hence, by remembering that the highest mode has order M, we see that a UCA needs to employ at least $N > 2M$ elements. Notice that this condition is similar to the Nyquist sampling criterion in which M defines the maximum spatial frequency component in the array excitation. This constraint could be too demanding for certain applications. For example a UCA of radius $r = \lambda$ and $M = 6$ requires that the array should have $N > 12$ sensors. In [16], it is suggested that, with some mathematical manipulation, it is possible to relax the constraint to $N \geq M$.

In order to avoid spatial aliasing or grating lobes in ULA, the spacing d between the array elements has to be less than 0.5λ [2], [5]. A common practice in designing arrays is to limit the interelement spacing to $0.3\lambda \leq d \leq 0.5\lambda$. The lower bound is defined by practical construction since the array elements have a certain physical size and they cannot overlap. Moreover, mutual coupling effects become more severe if the elements are too close.

IV. BEAMSPACE AND MODIFIED BEAMSPACE TRANSFORM

The BT [2] is a modal transform that maps the steering vectors of UCA into the steering vectors of a ULA-type array, called virtual array, with Vandermonde structure. This transform allows us to employ widely used computationally efficient methods originally designed for ULA also for UCA, e.g., root-MUSIC, ESPRIT, and spatial smoothing [2], [4], [7], [8].

The MBT improves the BT by providing a link between the residual term defined by the phase-mode excitation principle, in (7), and the residual error that arises when the BT is applied. Since the beamspace transform is based on the phase-mode excitation principle, the mapping between the UCA and the virtual

array steering vectors is approximate, and bias may be present in DoA estimates.

A. Beamspace Transform

The beamspace transform is done by employing a beamformer $\mathbf{F}_e^H$ (see [2] for details) as

$$\mathbf{a}_e(\boldsymbol{\vartheta}) = \mathbf{F}_e^H \mathbf{a}(\boldsymbol{\vartheta}) = \mathbf{C}_v \mathbf{V}^H \mathbf{a}(\boldsymbol{\vartheta}) \approx \sqrt{N}\mathbf{J}_\zeta \mathbf{d}(\phi) \tag{8}$$

where

$$\mathbf{C}_v = \mathrm{diag}\{j^{-M}, \ldots, j^{-1}, j^0, j^{-1}, \ldots, j^{-M}\} \tag{9}$$

$$\mathbf{V} = \sqrt{N}[\mathbf{w}_{-M} \vdots \cdots \vdots \mathbf{w}_0 \vdots \cdots \vdots \mathbf{w}_{-M}] \tag{10}$$

$$\mathbf{J}_\zeta = \mathrm{diag}\{J_M(\zeta), \ldots, J_1(\zeta), J_0(\zeta), J_1(\zeta), \ldots, J_M(\zeta)\} \tag{11}$$

$$\mathbf{d}(\phi) = [e^{-jM\phi}, \ldots, e^{-j\phi}, 1, e^{j\phi}, \ldots, e^{jM\phi}]^T. \tag{12}$$

The modes that can be excited are $m \in [-M, M]$, and $\mathcal{M} = 2M + 1$ is the total number of excited modes. The matrices $\mathbf{C}_v$ and $\mathbf{J}_\zeta$ are $\mathcal{M} \times \mathcal{M}$ diagonal matrices, the vector $\mathbf{d}(\phi)$ has size $\mathcal{M} \times 1$, the columns of the $N \times \mathcal{M}$ matrix $\mathbf{V}$ are defined as in (5), and $\mathrm{diag}\{\cdot\}$ denotes a diagonal matrix. It is interesting to note that vector $\mathbf{d}(\phi)$ is in the same form as in Vandermonde matrix and depends only on the azimuth angle ϕ. The transformation is an approximation since the term $\sqrt{N}\mathbf{J}_\zeta \mathbf{d}(\phi)$ is equal to $\mathbf{a}_e(\boldsymbol{\vartheta})$ when certain conditions (number of elements, interelement spacing, etc.) are fulfilled [2]. This is caused by the residual error.

In Section VI-A, we discuss how to minimize the residual term by choosing a suitable configuration of the UCA parameters. However, a small residual error term still remains after the BT. It can significantly deteriorate the performance of the DoA algorithms; see Section VI-B.

B. Modified Beamspace Transform

Given the beamformer defined by (8)–(12) and the UCA element-space steering vector $\mathbf{a}(\boldsymbol{\vartheta})$, the beamspace steering vector $\mathbf{a}_e(\boldsymbol{\vartheta})$ can be written as

$$\begin{aligned}\mathbf{a}_e(\boldsymbol{\vartheta}) &= \mathbf{F}_e^H \mathbf{a}(\boldsymbol{\vartheta}) = \mathbf{C}_v \mathbf{V}^H \mathbf{a}(\boldsymbol{\vartheta}) = \sqrt{N}\mathbf{J}_\zeta \mathbf{d}(\phi) + \sqrt{N}\mathbf{C}_v \boldsymbol{\varepsilon} \\ &= \sqrt{N}\mathbf{J}_\zeta(\mathbf{d}(\phi) + \boldsymbol{\Delta}\mathbf{d}_1(\phi) + O(\boldsymbol{\Delta}\mathbf{d}_2(\phi)))\end{aligned} \tag{13}$$

where

$$\boldsymbol{\Delta}\mathbf{d}_1(\phi) = \mathbf{J}_\zeta^{-1}\mathbf{C}_v \boldsymbol{\varepsilon}^{(1)} \tag{14}$$

with $\boldsymbol{\varepsilon}^{(1)} = [\varepsilon_{-M}^{(1)}, \ldots, \varepsilon_0^{(1)}, \ldots, \varepsilon_M^{(1)}]^T$. Here $\boldsymbol{\varepsilon}^{(1)}$ is defined according to (7) for $q = 1$ and $O(\boldsymbol{\Delta}\mathbf{d}_2(\phi))$ contains all the remaining terms of the sum $\boldsymbol{\varepsilon}^{(q)}$ for $q = 2, 3, \ldots, +\infty$. See also Appendix I.

As a result, we can now decompose the UCA beamspace steering vector into a sum of three vectors: $\mathbf{d}(\phi)$ is the steering vector of the virtual array with Vandermonde structure, $\boldsymbol{\Delta}\mathbf{d}_1(\phi)$ is an additive perturbation [10] with angular dependence on the nominal value of $\mathbf{d}(\phi)$, and $O(\boldsymbol{\Delta}\mathbf{d}_2(\phi))$ captures the remaining error that includes the components with a significantly smaller numerical value compared to the dominant term; see Table I. Notice that neglecting the latter terms does not cause any loss of generality because the discussion can be extended by including more terms. Consequently, the virtual array resulting from applying the beamspace transformation can be considered to be an array with a misplacement of the element position proportional to the residual error $\boldsymbol{\Delta}\mathbf{d}(\phi) = \boldsymbol{\Delta}\mathbf{d}_1(\phi)$.

It is interesting to notice that the perturbation in the elements location depends on the actual DoA. The transformation produces this residual error whenever the residual term defined by the phase-mode excitation principle appears. The residual error then introduces error in DoA estimates, i.e., bias or additional variance when beamspace methods are applied. In order to reduce the error in the DoA estimates, we derive a method for reducing the residual error in advance; see Section VII. In fact, it is a procedure for calibrating the virtual array automatically.

V. Impact of the Residual Error on the Signal and Noise Subspaces

Here the MBT is used for deriving a first-order approximation of the bias that is present in the DoA estimates when beamspace methods are applied on UCA. In particular we will focus on rooting techniques, such as root-MUSIC [2], [4]. The following analysis shows how the perturbation $\boldsymbol{\Delta}\mathbf{d}(\phi)$ will affect the array covariance matrix and, consequently, the signal and the noise subspaces.

Recalling (13), the observed data $\mathbf{X}$ are mapped from element space to beamspace as

$$\mathbf{Y} = \mathbf{F}_e^H \mathbf{X} = [\sqrt{N}\mathbf{J}_\zeta(\mathbf{d}(\phi) + \boldsymbol{\Delta}\mathbf{d}(\phi))]\mathbf{S} + \mathbf{F}_e^H \mathbf{N} \tag{15}$$

where, similarly to (13), we have neglected the small terms $O(\boldsymbol{\Delta}\mathbf{d}_2(\phi))$ and rewritten $\boldsymbol{\Delta}\mathbf{d}_1(\phi)$ as $\boldsymbol{\Delta}\mathbf{d}(\phi)$.

The array covariance matrix $\mathbf{R}_y = E\{\mathbf{y}(t)\mathbf{y}^H(t)\}$ may be expressed in terms of eigenvalue decomposition (see [10] for details)

$$\begin{aligned}\mathbf{R}_y = \tilde{\mathbf{E}}\tilde{\boldsymbol{\Lambda}}\tilde{\mathbf{E}}^H &= (\mathbf{E}_s + \boldsymbol{\Delta}\mathbf{E}_s)(\boldsymbol{\Lambda}_s + \boldsymbol{\Delta}\boldsymbol{\Lambda}_s)(\mathbf{E}_s + \boldsymbol{\Delta}\mathbf{E}_s)^H \\ &\quad + \sigma_\eta^2(\mathbf{E}_\eta + \boldsymbol{\Delta}\mathbf{E}_\eta)(\mathbf{E}_\eta + \boldsymbol{\Delta}\mathbf{E}_\eta)^H\end{aligned} \tag{16}$$

where $\tilde{\mathbf{E}}_s = \mathbf{E}_s + \boldsymbol{\Delta}\mathbf{E}_s$ denote perturbed signal subspace eigenvectors and $\mathbf{E}_s$ and $\boldsymbol{\Delta}\mathbf{E}_s$ denote the true signal subspace eigenvectors and the perturbation, respectively. In an analogous way, we express the noise subspace $\tilde{\mathbf{E}}_\eta = \mathbf{E}_\eta + \boldsymbol{\Delta}\mathbf{E}_\eta$ and the eigenvalues associated with the signal subspace as $\tilde{\boldsymbol{\Lambda}}_s = \boldsymbol{\Lambda}_s + \boldsymbol{\Delta}\boldsymbol{\Lambda}_s$. Note that for our purposes, we only consider perturbations due to transformation error. Another example of analyzing bias in the context of array interpolation can be found in [17]. The approach requires sectorization of the array, which is not needed in the method proposed in this paper.

From (16), and by considering (8), (13), and (15), we get the following orthogonality relationships for all $i = 1, \ldots, P$:

$$[\sqrt{N}\mathbf{J}_\zeta \mathbf{d}(\phi_i)]^H \tilde{\mathbf{E}}_\eta \neq 0 \tag{17}$$

$$[\sqrt{N}\mathbf{J}_\zeta \mathbf{d}(\phi_i)]^H \mathbf{E}_\eta = 0 \tag{18}$$

$$[\sqrt{N}\mathbf{J}_\zeta(\mathbf{d}(\phi_i) + \boldsymbol{\Delta}\mathbf{d}(\phi_i))]^H \tilde{\mathbf{E}}_\eta = 0. \tag{19}$$

Equation (16) shows that the residual error (or the perturbation vector $\boldsymbol{\Delta}\mathbf{d}(\phi)$) influences both signal and noise subspaces. This is an interesting result because it may also be used to justify the

differences in asymptotical performances of beamspace-based MUSIC and root-MUSIC algorithms for UCA. In fact, by implementing beamspace MUSIC, we implicitly consider the effect of the perturbation by using the perturbed noise subspace $\tilde{\mathbf{E}}_\eta$ in the entire derivation of the algorithm. Instead, in deriving the root-MUSIC for UCA, we first estimate the perturbed noise subspace in (16), but then we look for the orthogonality between $\mathbf{d}\perp\tilde{\mathbf{E}}_\eta$ instead of between $(\mathbf{d}+\boldsymbol{\Delta}\mathbf{d})\perp\tilde{\mathbf{E}}_\eta$.

A. Analysis of the Bias in the DoA Estimates

In order to analyze the bias introduced to DoA estimates, we will consider the UCA unitary root-MUSIC algorithm [4]. However, this does not limit the generality of the results since the same kind of procedure can be applied to different beamspace DoA estimation algorithms only by defining an appropriate expression for each of them. In the literature, another example of DoA bias analysis for array interpolation techniques can be found in [17].

The quadratic expression used in UCA unitary root-MUSIC is

$$\tilde{f}(\phi)=\mathbf{d}^H(\phi)\sqrt{N}\mathbf{J}_\zeta\mathbf{Q}_\mathcal{M}\tilde{\mathbf{E}}_\eta\tilde{\mathbf{E}}_\eta^H\mathbf{Q}_\mathcal{M}^H\sqrt{N}\mathbf{J}_\zeta\mathbf{d}(\phi) \tag{20}$$

and the P roots closest to the unit circle have to be found in order to estimate the DoAs [3], [4]. Here $\mathbf{Q}_\mathcal{M}$ is an $\mathcal{M}\times\mathcal{M}$ (where $\mathcal{M}$ is the size of the virtual array) unitary square column conjugate symmetric matrix; see [4] and [12] for construction. Since UCA unitary root-MUSIC works in a unitary beamspace domain, we will consider the unitary beamspace manifold formed by multiplying the left-hand side of (13) by $\mathbf{Q}_\mathcal{M}$

$$\begin{aligned}\mathbf{a}_u(\boldsymbol{\vartheta})&=\mathbf{Q}_\mathcal{M}^H\mathbf{F}_e^H\mathbf{a}(\boldsymbol{\vartheta})=\sqrt{N}\mathbf{Q}_\mathcal{M}^H\mathbf{J}_\zeta\mathbf{d}(\phi)+\sqrt{N}\mathbf{Q}_\mathcal{M}^H\mathbf{C}_v\boldsymbol{\varepsilon}^{(1)}\\&=\sqrt{N}\mathbf{J}_\zeta(\mathbf{Q}_\mathcal{M}^H\mathbf{d}(\phi)+\boldsymbol{\Delta}\mathbf{d}_u(\phi))\end{aligned} \tag{21}$$

where $\boldsymbol{\Delta}\mathbf{d}_u(\phi)=\mathbf{Q}_\mathcal{M}^H\mathbf{J}_\zeta^{-1}\mathbf{C}_v\boldsymbol{\varepsilon}^{(1)}$.

Our goal is then to establish a link between the residual term (or the element misplacement error) in the virtual array manifold and the perturbation in the noise subspace $\boldsymbol{\Delta}\mathbf{E}_\eta$. As in [11], we define

$$\mathbf{R}_y\tilde{\mathbf{E}}_\eta=\sigma_\eta^2\tilde{\mathbf{E}}_\eta \tag{22}$$

obtained by multiplying (16) from the right by $\tilde{\mathbf{E}}_\eta$. By using the derivation in [11], we can write the first-order approximation

$$\mathbf{E}_\eta\boldsymbol{\Delta}\mathbf{E}_\eta^H\mathbf{Q}_\mathcal{M}^H\mathbf{J}_\zeta\mathbf{d}(\phi)\sqrt{N}\approx-\mathbf{E}_\eta\mathbf{E}_\eta^H\boldsymbol{\Delta}\mathbf{d}_u(\phi). \tag{23}$$

Thus, from (23), we can conclude that the projection of the exact virtual array manifold $\sqrt{N}\mathbf{Q}_\mathcal{M}^H\mathbf{J}_\zeta\mathbf{d}(\phi)$ into the perturbed noise subspace is approximately equal to the projection of the perturbed virtual array manifold $\boldsymbol{\Delta}\mathbf{d}_u(\phi)$ into the exact noise subspace [11].

An expression for the bias can be found by expanding the first derivative of the (20) with respect to ϕ_i and evaluating at the estimate $\hat{\phi}_i$. As in [11] and [13], for small enough errors, we can write

$$0=\tilde{f}'(\hat{\phi}_i)\approx\tilde{f}'(\phi_i)+\tilde{f}''(\phi_i)(\hat{\phi}_i-\phi_i) \tag{24}$$

where ϕ_i and $\hat{\phi}_i$ are the true and estimated DoA for the ith source and $\tilde{f}'(\hat{\phi}_i)\triangleq(\partial\tilde{f}(\phi))/(\partial\phi)\big|_{\phi=\hat{\phi}_i}$.

In order to solve (24) with respect to the error term $(\hat{\phi}_i-\phi_i)$, we have to define the $\mathcal{M}\times 1$ vector $\mathbf{v}(\phi)$ as

$$\mathbf{v}(\phi)\triangleq\frac{\partial\mathbf{d}(\phi)}{\partial\phi}=\begin{bmatrix}-jMe^{-jM\phi}\\-j(M-1)e^{-j(M-1)\phi}\\\vdots\\0\\\vdots\\j(M-1)e^{j(M-1)\phi}\\jMe^{jM\phi}\end{bmatrix} \tag{25}$$

and then to compute the first and second derivative of (20).

The first derivative of the expression is calculated as [11]

$$\begin{aligned}\tilde{f}'(\phi)&=\frac{\partial\tilde{f}(\phi)}{\partial\phi}\\&=2\Re\Big\{N\mathbf{v}^H(\phi)\mathbf{J}_\zeta\mathbf{Q}_\mathcal{M}\tilde{\mathbf{E}}_\eta\tilde{\mathbf{E}}_\eta^H\mathbf{Q}_\mathcal{M}^H\mathbf{J}_\zeta\mathbf{d}(\phi)\Big\}\end{aligned} \tag{26}$$

where $\Re\{\cdot\}$ stands for the real part of the argument within the brackets. Equation (26) can be rewritten by considering first that $\tilde{\mathbf{E}}_\eta=\mathbf{E}_\eta+\boldsymbol{\Delta}\mathbf{E}_\eta$, second that $\sqrt{N}\mathbf{d}^H(\phi)\mathbf{J}_\zeta\mathbf{Q}_\mathcal{M}\mathbf{E}_\eta=0$, and third that we are looking for a first-order approximation where all the higher order terms such as $O(\|\boldsymbol{\Delta}\mathbf{E}\|^2)$ are neglected. As a result, we get

$$\tilde{f}'(\phi)\approx2\Re\big\{N\mathbf{v}^H(\phi)\mathbf{J}_\zeta\mathbf{Q}_\mathcal{M}\mathbf{E}_\eta\boldsymbol{\Delta}\mathbf{E}_\eta^H\mathbf{Q}_\mathcal{M}^H\mathbf{J}_\zeta\mathbf{d}(\phi)\big\} \tag{27}$$

which according to (23) can be expressed as

$$\tilde{f}'(\phi)\approx2\Re\Big\{-\mathbf{v}^H(\phi)\sqrt{N}\mathbf{J}_\zeta\mathbf{Q}_\mathcal{M}\mathbf{E}_\eta\mathbf{E}_\eta^H\boldsymbol{\Delta}\mathbf{d}_u(\phi)\Big\}. \tag{28}$$

In (24), we notice that the second derivative of the cost function is multiplied by the error term $(\hat{\phi}_i-\phi_i)$ that is assumed to be small [11]. Therefore, we can make the first-order approximation $\tilde{f}''(\phi_i)(\hat{\phi}_i-\phi_i)\approx f''(\phi_i)(\hat{\phi}_i-\phi_i)$ and find the second derivative as follows:

$$f''(\phi)=\frac{\partial f'(\phi)}{\partial\phi}=2N\mathbf{v}^H(\phi)\mathbf{J}_\zeta\mathbf{Q}_\mathcal{M}\mathbf{E}_\eta\mathbf{E}_\eta^H\mathbf{Q}_\mathcal{M}^H\mathbf{J}_\zeta\mathbf{v}(\phi) \tag{29}$$

where $f'(\phi)$ represents (26) computed by considering the true noise subspace $\mathbf{E}_\eta$. By combining (24), (28), and (29), an expression for the bias for the DoA estimates at angle ϕ_i can finally be written as

$$\hat{\phi}_i-\phi_i\approx\frac{\Re\big\{-\mathbf{v}^H(\phi_i)\mathbf{J}_\zeta\mathbf{Q}_\mathcal{M}\mathbf{E}_\eta\mathbf{E}_\eta^H\boldsymbol{\Delta}\mathbf{d}_u(\phi_i)\big\}}{\sqrt{N}\mathbf{v}^H(\phi_i)\mathbf{J}_\zeta\mathbf{Q}_\mathcal{M}\mathbf{E}_\eta\mathbf{E}_\eta^H\mathbf{Q}_\mathcal{M}^H\mathbf{J}_\zeta\mathbf{v}(\phi_i)}. \tag{30}$$

Fig. 4 illustrates the bias term in (30) that arises when UCA unitary root-MUSIC algorithm is applied to a UCA with a small

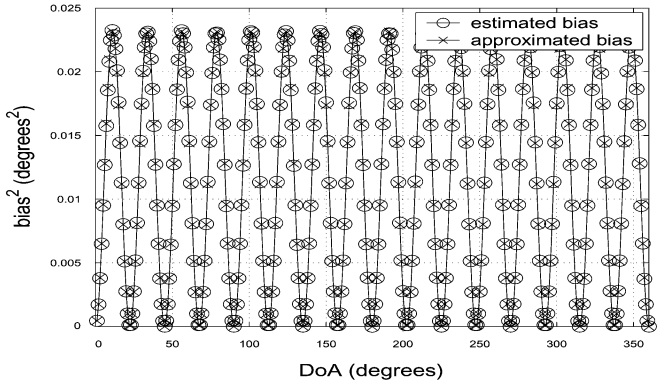

Fig. 4. Comparison between the estimated bias provided by UCA unitary root-MUSIC and the first-order approximation of the bias term. The approximation appears to be accurate since the curves overlap. The bias depends on the DoA.

number of sensors. In the simulation we used one source moving in the range $\phi \in [0, 2\pi)$, $N = 8$ sensors, array radius $r = (\lambda/2.6), K = 256$ snapshots, signal-to-noise ratio (SNR) $=$ 50 dB, and 100 independent Monte Carlo trials. Here, we can also notice the angular dependence of the bias as a direct consequence of the angular dependence of the residual error. We can easily see that the first-order approximation derived in this paper describes the bias with high fidelity. It provides *a priori* information on the bias present on the DoA estimates at angle ϕ_i and provides means for removing the bias, as described in Section VII.

Fig. 5 depicts the performance of UCA unitary root-MUSIC in terms of MSE. Notice that as the SNR increases, the variance on the estimates decreases and, for very large values of SNR (asymptotically), just a bias term is still present on the estimates. This appears as an error floor that is well described by the bias term in (30).

VI. Error in Different UCA Configurations

A. Quantitative Analysis of the Residual Term

We analyze the behavior of the residual term as a function of different UCA configuration parameters. We provide some rules of thumbs for the designer of a UCA in order to find the best tradeoff among the array parameters (number of sensors, radius, interelement spacing), which leads to tolerable residual error. Unfortunately, choosing appropriate configuration parameters may not be sufficient for avoiding biased DoA estimates when rooting algorithms for UCA are used. Some additional techniques are needed.

An example of bias reduction can be found in [17], where an optimal mapping from circular to linear manifold is proposed. However, this method splits the range of azimuthal angles in sectors of 30° and processes each sector separately.

In general, it is obvious that the closer we get to a continuous array configuration, the smaller the residual term will be. We could assume that the residual term in (7) can be considered "small enough" if $\varepsilon_m \leq 0.01$ as suggested in [2].

In Fig. 6, we have plotted residual terms of Mth order as a function of the radius for arrays with different number of sensors. The residual terms were formed first by setting $q = 1$ and

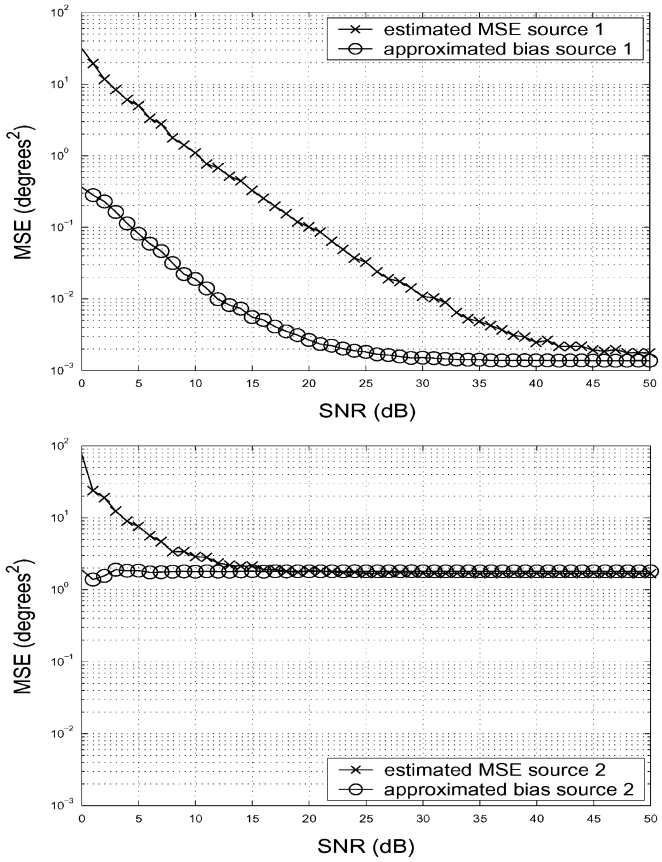

Fig. 5. Comparison between the estimated MSE of UCA unitary root-MUSIC and the first-order approximation of the squared bias term. For large values of SNR curves overlap. Settings: $N = 8, r = (\lambda/2.6), K = 500$, two uncorrelated sources at $(\phi_1, \phi_2) = (10°, 25°)$, and 1000 independent Monte Carlo trials.

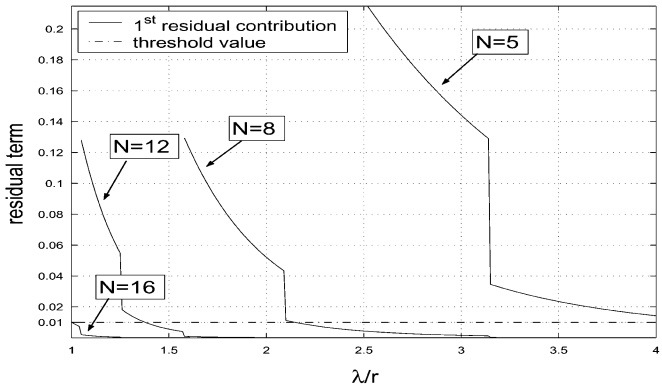

Fig. 6. Residual term as function of the UCA radius for different number of sensors. The residual value 0.01 is the threshold under which the residual error is considered to be negligible.

$m = M$ in (7) and then by considering UCAs with different numbers of sensors. It is interesting to notice that since M is proportional to r (the smallest integer close or equal to κr) the discontinuities in the functions appear every time the value of M decreases. Note that due to the constraint on the maximum interelement spacing (Section III-B), large values of $\lambda \backslash r$ are not of practical interest. In Fig. 7, we have numerical results showing the dependence of the residual term on both the number of sensors and the radius.

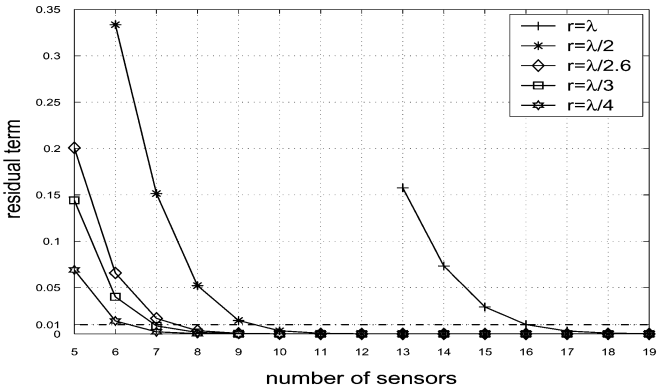

Fig. 7. Evaluation of the residual term. For fixed number of sensors the residual term grows as the UCA radius increases. For a fixed radius, however, it decreases as the number of sensors increases.

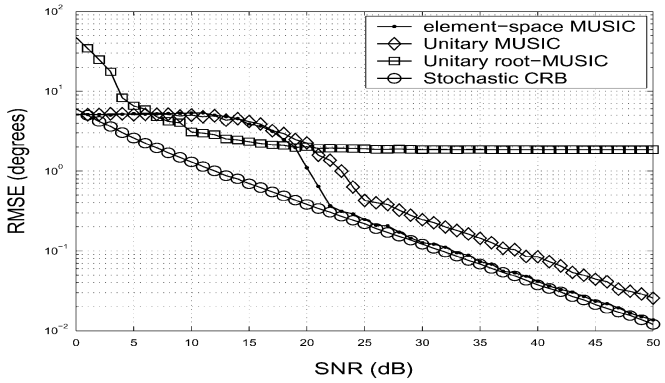

Fig. 8. RMSE of the DoA algorithms compared to CRB when a UCA with a small number of sensors is used. Only unitary root-MUSIC suffers from bias. Settings: $N = 8, r = (\lambda/2.6), d = 0.2944\lambda, K = 256$ and the uncorrelated sources located at $(\phi_1, \phi_2) = (10^\circ, 20^\circ)$.

B. Effects of the Residual Error on the DoA Estimates

The DoA estimators for UCA work either in element space (processing directly the data recorded by the array) or in beamspace [2], [4], [7], [8] (preprocessing the data by the beamspace transform).

From a theoretical point of view, the asymptotic performance of element-space methods is better than beamspace methods. In fact, it has been proved [6] that the variance of the estimates is always less than the variance obtained by working in the beamspace domain. For uncorrelated signals, the element-space version of MUSIC achieves the CRB for reasonably large values of N, K, or SNR [13], [14].

On the other hand, working in beamspace provides advantages because it allows the reconstruction of the Vandermonde structure of the UCA steering vectors. Hence, widely used techniques for ULA such as root-MUSIC [2], [4] and spatial smoothing [7], [8] may be used as UCA configurations as well.

In the class of algorithms that employ the beamspace transform, significant difference in performance can be observed depending on how the transformation is applied. Let us recall the key idea of (13): by multiplying from the left the UCA steering vector $\mathbf{a}(\boldsymbol{\vartheta})$ by an appropriate beamformer (in this case $\mathbf{F}_e$), we map the array manifold from the element-space to the beamspace domain. The beamspace steering vector $\mathbf{a}_e(\boldsymbol{\vartheta})$ can then be defined either as $\mathbf{F}_e^H \mathbf{a}(\boldsymbol{\vartheta})$ or as the sum of $\sqrt{N}\mathbf{J}_\zeta \mathbf{d}(\phi) + \sqrt{N}\mathbf{C}_v\boldsymbol{\varepsilon}$, where the second term is the residual error that arises after the transformation.

Algorithms such as UCA-RB-MUSIC or UCA unitary MUSIC [2], [4] are implemented only by employing the $\mathbf{F}_e^H \mathbf{a}(\boldsymbol{\vartheta})$ expression of the beamspace manifold. For this reason, they do not suffer from the bias created by the residual error. They show only a larger variance in the DoA estimates [6], [19]. On the other hand, algorithms like UCA-RB-root-MUSIC or UCA unitary root-MUSIC [2], [4] require both representations of the manifold $\mathbf{a}_e(\boldsymbol{\vartheta})$ throughout the implementation. However, since the residual error is not taken into account and only $\mathbf{a}_e(\boldsymbol{\vartheta}) \approx \sqrt{N}\mathbf{J}_\zeta \mathbf{d}(\phi)$ is used, this leads to biased estimates. A systematic error in the DoA estimates is introduced.

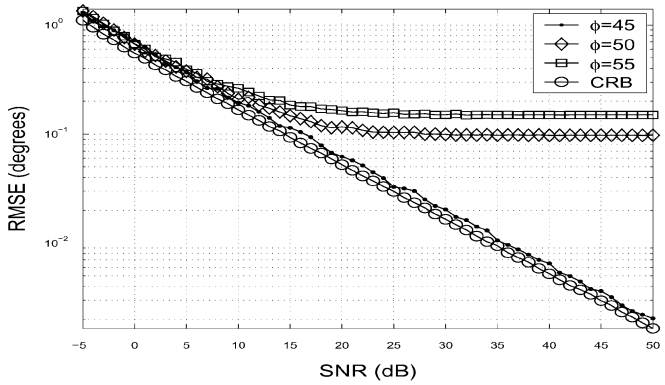

Fig. 9. Statistical performances of UCA unitary root-MUSIC algorithms for different source angles compared to the stochastic CRB. The bias in the DoA estimates clearly depends on the angle of arrival. Settings: $N = 8$ sensors, interelement spacing $d = 0.3\lambda$, and $K = 256$ snapshots.

Consequently, beamspace-based MUSIC and root-MUSIC algorithms for UCAs have difference in asymptotic performances (both for large sample size and for high SNR), whereas in the case of ULA, the performances are identical [15].

In Fig. 8, the differences between working in element-space or in beamspace domain are clearly illustrated. Also the difference in performances between the beamspace-based MUSIC and root-MUSIC implementation is evident.

In Fig. 9, the effect of the residual error on the performance of UCA unitary root-MUSIC is depicted. The bias introduced by the residual error causes an error floor and, since the residual term and the residual error depend on the DoA, the bias shows a clear angular dependence, which has a significant impact on the statistical performance.

C. Bias in Case of Even or Odd Number of Elements

An interesting observation is presented next. The UCA root-MUSIC algorithm gives almost bias-free estimates when an odd number of sensors is used. Otherwise, a biased term as in (30) appears.

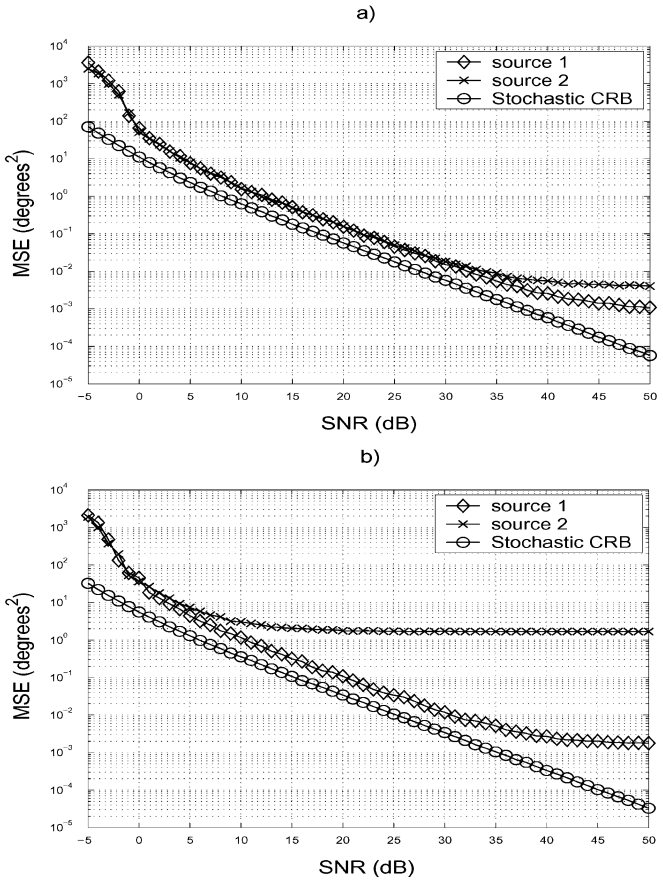

Fig. 10. Statistical performances of DoA algorithms for UCA when an (a) odd or (b) even small number of sensors is used. Bias appears as an error floor. Settings: $N = 7$ in (a) and $N = 8$ in (b) sensors, $d = 0.3\lambda, K = 500$, and two uncorrelated sources located at $(\phi_1, \phi_2) = (10^\circ, 25^\circ)$.

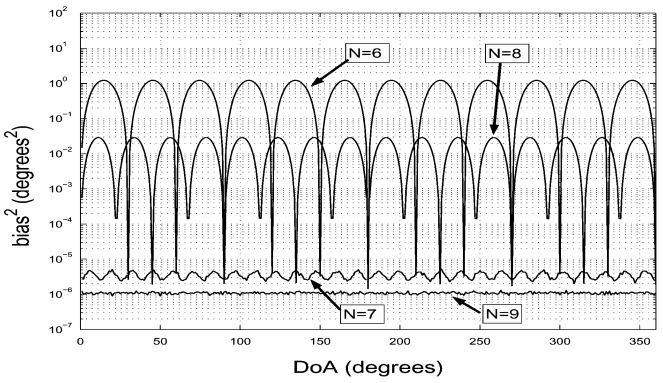

Fig. 11. Bias as function of the DoAs computed with UCA unitary root-MUSIC when different number of sensors are used. Settings: $K = 500$, SNR $= 50$ dB, and interelement spacing $d = 0.3\lambda$. Note that arrays with odd number of elements have lower bias.

This is depicted in Fig. 10 where two effective examples are shown. In Fig. 10(a) we have a UCA with an odd number of sensors, while in (b) a configuration with an even number is considered. Clearly, a significant reduction in bias appears by using seven instead of eight sensors.

A more general example describing the effect of the number of sensors in UCA on the asymptotical MSE of a DoA estimator

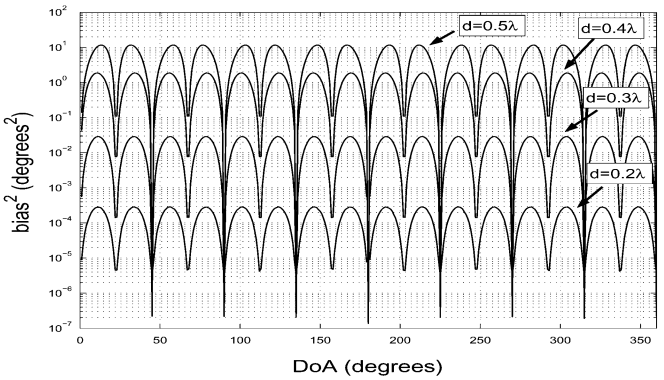

Fig. 12. Bias on the estimates of UCA unitary root-MUSIC as function of the DoAs for several interelement spacing d when $N = 8$ sensors are used. Settings: $K = 500$, SNR $= 50$ dB. Note that the bias increases as the interelement spacing increases.

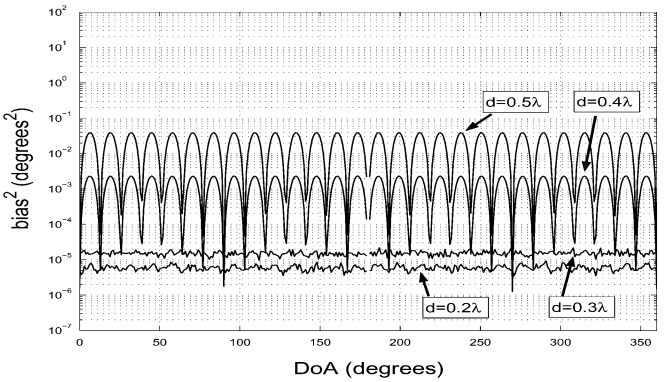

Fig. 13. Bias on the estimates of UCA unitary root-MUSIC as function of the DoAs when $N = 7$ sensors are used. Settings: $K = 500$, SNR $= 50$ dB, and several interelement spacing d.

is shown in Fig. 11. Note that for large values of SNR, the bias forms an error floor and becomes dominant compared to the variance. This further demonstrates the fact that employing the beamspace transform on an UCA with an odd number of sensors may provide DoA estimates with lower bias. We can also notice that the period of the oscillations is inversely proportional to N. In Figs. 12 and 13, we depict the dependence of the bias on different interelement spacings both for configurations with even and odd number of sensors. In the case of odd number of elements, the bias is about three orders of magnitude smaller than with an even number of elements. The plots also show that the period of oscillations does not depend on the interelement spacing, while the amplitude of the bias is directly proportional to d.

All the curves representing the behavior of the bias for UCA configurations with an even number of sensors can be described by using (30). In the case of an odd number of elements, the first-order approximation may not be sufficient and a second-order approximation should be used instead. On the other hand, the bias error is very small then and does not significantly affect the DoA estimates.

A theoretical justification of the prediction power of our first-order approximation can be easily found by analyzing (30). The

denominator is a quadratic function and may be characterized as a function $\mathcal{D}$: $\mathbb{C}^N \longrightarrow \mathbb{R}$. On the other hand, the numerator of (30) (without considering the real part) is a function $\mathcal{N}$: $\mathbb{C}^N \longrightarrow \mathbb{R}$ if N is even and $\mathbb{C}^N \longrightarrow \mathbb{C}$ if N is odd. This is due to the construction of the vectors $\mathbf{\Delta d}_u(\phi)$ [see (21)], and in particular to how the $\mathcal{M} \times 1$ vector $\boldsymbol{\varepsilon}$ is formed [see (13)]. Observe that $\mathcal{M} = 2M + 1$ is by definition always an odd number. The element of $\boldsymbol{\varepsilon}$ related to $m = 0$ and $q = 1$ is $\varepsilon_0^{(1)}$ and is defined as $j^N J_N(\zeta)e^{-jN\phi} + j^N J_N(\zeta)e^{jN\phi} = 2j^N J_N(\zeta)\Re\{e^{-jN\phi}\}$; see (7) and (13). We notice that $\varepsilon_0^{(1)}$ is a pure imaginary number when N is odd. Consequently, for N odd, the numerator of (30) is purely imaginary and we may conclude in the first-order approximation that the bias term on the DoA estimates (caused by the residual error in the BT) is negligible.

VII. Algorithm for Bias Reduction

In this section, we derive the beamformers $\mathbf{F}_{e1}^H$ and $\mathbf{F}_{e2}^H$ that are able to synthesize the dominant term of the residual error (for $q = 1$); see (7) and (13). This allows us to develop a three-step technique for bias removal on the DoA estimates. Note that since the bias depends on the DoA, it cannot be removed in advance.

The MBT defined in Section IV-B provides an expression of the residual errors $\sqrt{N}\mathbf{C}_v\boldsymbol{\varepsilon}$ where $\boldsymbol{\varepsilon}$ is the $\mathcal{M}\times$ 1 vector that contains the residual terms; see (7) and (31), shown at the bottom of the page. As discussed in Section III-B and Table I, the first term of each sum (for $q = 1$, where q is the index of the sum) is several orders of magnitude larger than the remaining terms, for $q \geq 2$. Hence, only the dominant terms of the sums will be considered in the following discussion. By taking the first $(q = 1)$ term of each sum, the dominant residual term in (31) can be split into two components $\boldsymbol{\varepsilon}^{(1)} = \boldsymbol{\varepsilon}_1^{(1)} + \boldsymbol{\varepsilon}_2^{(1)}$, where

$$\boldsymbol{\varepsilon}_1^{(1)} = \begin{bmatrix} j^{(N+M)}J_{(N+M)}(\zeta)e^{-j(N+M)\phi} \\ j^{(N+M-1)}J_{(N+M-1)}(\zeta)e^{-j(N+M-1)\phi} \\ \vdots \\ j^N J_N(\zeta)e^{-jN\phi} \\ \vdots \\ j^{(N-M+1)}J_{(N-M+1)}(\zeta)e^{-j(N-M+1)\phi} \\ j^{(N-M)}J_{(N-M)}(\zeta)e^{-j(N-M)\phi} \end{bmatrix} \quad (32)$$

$$\boldsymbol{\varepsilon}_2^{(1)} = \begin{bmatrix} j^{(N-M)}J_{(N-M)}(\zeta)e^{j(N-M)\phi} \\ j^{(N-M+1)}J_{(N-M+1)}(\zeta)e^{j(N-M+1)\phi} \\ \vdots \\ j^N J_N(\zeta)e^{jN\phi} \\ \vdots \\ j^{(N+M-1)}J_{(N+M-1)}(\zeta)e^{j(N+M-1)\phi} \\ j^{(N+M)}J_{(N+M)}(\zeta)e^{j(N+M)\phi} \end{bmatrix} \quad (33)$$

which are the expressions for the dominant terms of the residual error; see (7) and (14).

The key idea is that by exploiting the concept of phase-mode excitation (Section III), we derive two new beamformers that are able to synthesize a beampattern according to (32) and (33). Note that this kind of approach proceeds in an opposite manner to the one represented in Section III. There we wanted to define the far-field patterns resulting from exciting the aperture with some excitation modes, while here we are interested in defining the excitation modes that describe the normalized far-field patterns as in (32) and (33).

We start by considering the continuous circular aperture case. Similarly to (3) and (4), we define the far-field patterns resulting from exciting the aperture with the mode $w_m^{(1)}(\gamma) = e^{j(m-N)\gamma}$ (with $\alpha = N - m$) as

$$j^\alpha J_\alpha(\zeta)e^{-j\alpha\phi} = \frac{1}{2\pi}\int_0^{2\pi} e^{j\zeta\cos(\phi-\gamma)}e^{j(m-N)\gamma}\,\mathrm{d}\gamma \quad (34)$$

and $w_m^{(2)}(\gamma) = e^{j(N+m)\gamma}$ (with $\beta = N + m$) as

$$j^\beta J_\beta(\zeta)e^{j\beta\phi} = \frac{1}{2\pi}\int_0^{2\pi} e^{j\zeta\cos(\phi-\gamma)}e^{j(N+m)\gamma}\,\mathrm{d}\gamma. \quad (35)$$

The outline of the derivation of (34)–(35) can be found in Appendix II. A numerical evaluation of the same integrals is given in Appendix III. For $m \in [-M, M]$, (34) and (35) describe the first and second component of vectors in (32) and (33).

Having the integrals in (34) and (35), the general idea in the algorithm for bias reduction is the following. The $N \times K$ element-space data matrix $\mathbf{X}$ is mapped into the $\mathcal{M}\times K$ beamspace data matrix $\mathbf{Y}$ by using the BT [2], [4]. Combining (1), (13), (32), and (33), we can write

$$\mathbf{Y} = \mathbf{F}_e^H\mathbf{X} = \mathbf{F}_e^H\mathbf{AS} + \mathbf{F}_e^H\mathbf{N} \quad (36)$$

$$\boldsymbol{\varepsilon} = \begin{bmatrix} \sum_{q=1}^{\infty}\left(j^{(Nq+M)}J_{(Nq+M)}(\zeta)e^{-j(Nq+M)\phi} + j^{(Nq-M)}J_{(Nq-M)}(\zeta)e^{j(Nq-M)\phi}\right) \\ \sum_{q=1}^{\infty}\left(j^{(Nq+M-1)}J_{(Nq+M-1)}(\zeta)e^{-j(Nq+M-1)\phi} + j^{(Nq-M+1)}J_{(Nq-M+1)}(\zeta)e^{j(Nq-M+1)\phi}\right) \\ \vdots \\ \sum_{q=1}^{\infty}\left(j^{(Nq)}J_{(Nq)}(\zeta)e^{-j(Nq)\phi} + j^{(Nq)}J_{(Nq)}(\zeta)e^{j(Nq)\phi}\right) \\ \vdots \\ \sum_{q=1}^{\infty}\left(j^{(Nq-M+1)}J_{(Nq-M+1)}(\zeta)e^{-j(Nq-M+1)\phi} + j^{(Nq+M-1)}J_{(Nq+M-1)}(\zeta)e^{j(Nq+M-1)\phi}\right) \\ \sum_{q=1}^{\infty}\left(j^{(Nq-M)}J_{(Nq-M)}(\zeta)e^{-j(Nq-M)\phi} + j^{(Nq+M)}J_{(Nq+M)}(\zeta)e^{j(Nq+M)\phi}\right) \end{bmatrix} \quad (31)$$

TABLE II
ALGORITHM FOR BIAS REDUCTION

Step 1: Form the array observation matrix $\mathbf{X}$ as in eq.(1),

a) compute the initial beamspace data matrix $\mathbf{Y}$ by using eq.(15)

b) estimate the initial set of DoAs by using UCA root-MUSIC algorithm [2],[4]

Step 2: with the initial DoAs computed on step 1

c) evaluate (50)-(51) and form $\varepsilon_1^{(1)}$ and $\varepsilon_2^{(1)}$ as in (32)-(33),

d) compute the estimated steering matrix $\mathbf{A}_R$ as in (2),

e) form the beamformers $\mathbf{F}_{e1}^H$ and $\mathbf{F}_{e2}^H$ by using equations (41)-(42),

f) compute the new beamspace data matrix $\hat{\mathbf{Y}}$ starting from the initial observation matrix $\mathbf{X}$ as in eq.(45),

g) using UCA root-MUSIC algorithm, estimate the second set of DoAs.

Step 3: with the DoAs computed on step 2

h) repeat the points (c), (d), (e) and (f),

i) estimate the unbiased DoAs by using the UCA root-MUSIC algorithm.

$$= \left(\sqrt{N}\mathbf{J}_\zeta \mathbf{d}(\phi) + \sqrt{N}\mathbf{C}_v\boldsymbol{\varepsilon}^{(1)}\right)\mathbf{S} + \mathbf{F}_e^H\mathbf{N} \quad (37)$$

$$= \sqrt{N}\left(\mathbf{J}_\zeta \mathbf{d}(\phi) + \mathbf{C}_v\boldsymbol{\varepsilon}_1^{(1)} + \mathbf{C}_v\boldsymbol{\varepsilon}_2^{(1)}\right)\mathbf{S} + \mathbf{F}_e^H\mathbf{N} \quad (38)$$

in which the two terms $(\sqrt{N}\mathbf{C}_v\boldsymbol{\varepsilon}_1^{(1)})\mathbf{S}$ and $(\sqrt{N}\mathbf{C}_v\boldsymbol{\varepsilon}_2^{(1)})\mathbf{S}$ related to the residual term of the BT have been written separately. The term $(\sqrt{N}\mathbf{J}_\zeta\mathbf{d}(\phi))\mathbf{S}$ forms the ideal beamspace data matrix given as a product of the ideal steering vector with Vandermonde structure $\mathbf{d}(\phi)$ and the signal $\mathbf{S}$. The noise term $\mathbf{F}_e^H\mathbf{N}$ remains a white complex circular Gaussian process since the beamformer matrix $\mathbf{F}_e^H$ is unitary.

Our goal is to remove $(\sqrt{N}\mathbf{C}_v\boldsymbol{\varepsilon}_1^{(1)})\mathbf{S}$ and $(\sqrt{N}\mathbf{C}_v\boldsymbol{\varepsilon}_2^{(1)})\mathbf{S}$ from (38) because they cause the bias. Clearly we do not know the terms since the signal matrix $\mathbf{S}$ is not known. An alternate solution is to construct two other beamformers $\mathbf{F}_{e1}^H$ and $\mathbf{F}_{e2}^H$ in order to synthesize the bias term and then simply cancel it out. The beamformers are

$$\mathbf{F}_{e1}^H\hat{\mathbf{A}} = \sqrt{N}\mathbf{C}_v\boldsymbol{\varepsilon}_1^{(1)} \quad (39)$$

$$\mathbf{F}_{e2}^H\hat{\mathbf{A}} = \sqrt{N}\mathbf{C}_v\boldsymbol{\varepsilon}_2^{(1)}. \quad (40)$$

The minimum-norm solution to (39) and (40) that defines the beamformers can be found as [18]

$$\mathbf{F}_{e1} = \hat{\mathbf{A}}^\dagger\sqrt{N}\boldsymbol{\varepsilon}_1^{(1)H}\mathbf{C}_v^H \quad (41)$$

$$\mathbf{F}_{e2} = \hat{\mathbf{A}}^\dagger\sqrt{N}\boldsymbol{\varepsilon}_2^{(1)H}\mathbf{C}_v^H \quad (42)$$

where $\hat{\mathbf{A}}$ is an estimated UCA element-space steering matrix with left pseudoinverse $\hat{\mathbf{A}}^\dagger = \hat{\mathbf{A}}(\hat{\mathbf{A}}^H\hat{\mathbf{A}})^{-1}$ and $\mathbf{C}_v$ is defined in (9). Note that $\hat{\mathbf{A}}$ cannot be directly computed because it would require knowledge of the DoAs. Equations (41) and (42) are instead computed by using an estimated steering matrix $\mathbf{A}_R$. For more details, see Table II.

At this point, we can form the correction data matrices as

$$\tilde{\mathbf{Y}}_1 = \mathbf{F}_{e1}^H\mathbf{X} = \left(\sqrt{N}\mathbf{C}_v\boldsymbol{\varepsilon}_1^{(1)}\right)\mathbf{S} + \mathbf{F}_{e1}^H\mathbf{N} \quad (43)$$

$$\tilde{\mathbf{Y}}_2 = \mathbf{F}_{e2}^H\mathbf{X} = \left(\sqrt{N}\mathbf{C}_v\boldsymbol{\varepsilon}_2^{(1)}\right)\mathbf{S} + \mathbf{F}_{e2}^H\mathbf{N} \quad (44)$$

where $\mathbf{X}$ is the UCA element-space data matrix.

The bias cancellation is performed by substituting the original beamspace data matrix $\mathbf{Y}$ by the two correction data matrices $\tilde{\mathbf{Y}}_1$ and $\tilde{\mathbf{Y}}_2$. Mathematically, we have

$$\hat{\mathbf{Y}} = \mathbf{Y} - \tilde{\mathbf{Y}}_1 - \tilde{\mathbf{Y}}_2 = \left(\mathbf{F}_e^H - \mathbf{F}_{e1}^H - \mathbf{F}_{e2}^H\right)\mathbf{X} \quad (45)$$

$$= \sqrt{N}\left(\mathbf{J}_\zeta\mathbf{d}(\phi) + \mathbf{C}_v\boldsymbol{\varepsilon}_1^{(1)} + \mathbf{C}_v\boldsymbol{\varepsilon}_2^{(1)}\right)\mathbf{S} + \mathbf{F}_e^H\mathbf{N} - \left(\sqrt{N}\mathbf{C}_v\boldsymbol{\varepsilon}_1^{(1)}\right)\mathbf{S} - \mathbf{F}_{e1}^H\mathbf{N} - \left(\sqrt{N}\mathbf{C}_v\boldsymbol{\varepsilon}_2^{(1)}\right)\mathbf{S} - \mathbf{F}_{e2}^H\mathbf{N}$$

$$= (\sqrt{N}\mathbf{J}_\zeta\mathbf{d}(\phi))\mathbf{S} + \left(\mathbf{F}_e^H - \mathbf{F}_{e1}^H - \mathbf{F}_{e2}^H\right)\mathbf{N} \quad (46)$$

where $\sqrt{N}\mathbf{J}_\zeta\mathbf{d}(\phi)$ is the ideal steering vector of the virtual array with Vandermonde structure. Notice that since the $\|\boldsymbol{\varepsilon}_1^{(1)}\|$ and $\|\boldsymbol{\varepsilon}_2^{(1)}\|$ are $\ll 1$, then $\|\mathbf{F}_{e1}^H\|$ and $\|\mathbf{F}_{e2}^H\|$ are $\ll 1$ too. This means that $(\mathbf{F}_e^H - \mathbf{F}_{e1}^H - \mathbf{F}_{e2}^H)$ is very close to unitary, i.e., $(\mathbf{F}_e^H - \mathbf{F}_{e1}^H - \mathbf{F}_{e2}^H)(\mathbf{F}_e^H - \mathbf{F}_{e1}^H - \mathbf{F}_{e2}^H)^H \approx \mathbf{I}$ because the two correction terms have a very small impact on the unitary matrix $\mathbf{F}_e^H$. Hence, we can say that the statistics of the noise does not change significantly and we may still consider the noise at this stage to be complex circular Gaussian process.

The bias reduction may be done in three steps: use the conventional BT for mapping the data from the element space to beamspace. Then compute the residual error by introducing two new beamformers $\mathbf{F}_{e1}^H$ and $\mathbf{F}_{e2}^H$. Finally, correct the original beamformer $\mathbf{F}_e^H$ by subtracting the new beamformers from the original one.

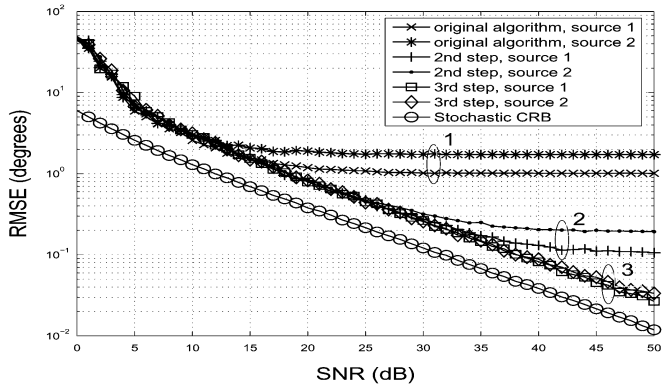

Fig. 14. Cancellation steps for the original UCA unitary root MUSIC algorithm, after the second iteration and after the third iteration. Settings: $N = 8, r = (\lambda/2.6), K = 256$, and $(\phi_1, \phi_2) = (15^\circ, 25^\circ)$.

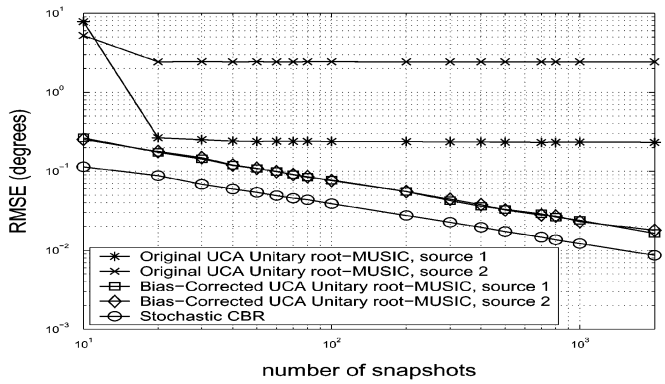

Fig. 15. Performances of the UCA unitary root-MUSIC algorithm. Settings: $N = 8, r = (\lambda/2.6)$, SNR $= 50$ dB and $(\phi_1, \phi_2) = (10^\circ, 15^\circ)$.

In Fig. 14, we show the decrease of the error in UCA unitary root-MUSIC algorithm in each step. The original DoA estimates are clearly biased, and two clear error floors are visible in the figure. After the second step, the two error floors are lowered significantly. Finally, after the third step, the bias is practically completely removed and no error floor occurs. In fact, the curves are parallel to the CRB. Observe that the algorithm does not achieve the CRB since the beamspace transform adds extra variance on the DoA estimates [6]. A method for reducing the excess variance is proposed in [19].

In Fig. 15, we depict the performance of UCA unitary root-MUSIC with the novel bias removal technique proposed in this paper. Significant improvement over the original technique where no bias reduction is applied is achieved. A summary of the proposed algorithm for bias removal is given in Table II.

VIII. Conclusion

In this paper, we provided an analysis of the systematic errors in the DoA estimates. It appears when the BT is applied to UCA configurations with small number of elements. Azimuth angle only is considered at a fixed elevation angle. The error and its dependence of array configuration parameters are characterized both qualitatively and quantitatively. First-order approximation of the bias in the DoA estimates is derived. An algorithm for removing the bias caused by the BT is proposed.

In this paper, a modified beamspace transform is introduced. It performs mapping from element space to beamspace by taking into account the error caused by the transform. It represents an exact expression for the transformation. The MBT leads to an interesting interpretation of the error: it can be considered as a misplacement error on the location of the sensors in the ULA-like virtual array.

Finally, the impact of the beamspace transform on two widely used DoA estimation algorithms for UCA is studied. The BT allows both computationally efficient DoA estimators and techniques able to deal with coherent sources to work for UCA as well. We demonstrate that beamspace-based MUSIC and root-MUSIC techniques for UCA have difference in their large sample properties. Moreover, the bias varies significantly depending on whether an even or odd number of elements are used in an UCA configuration.

Appendix I
Derivation of (13)

Let us recall (6) and (7). Then, by rewriting these in a matrix form for all excitation modes $m \in [-M, M]$, we get

$$\begin{bmatrix} \mathbf{w}_{-M}^H \\ \vdots \\ \mathbf{w}_0^H \\ \vdots \\ \mathbf{w}_M^H \end{bmatrix} \mathbf{a}(\boldsymbol{\vartheta}) = \operatorname{diag}\begin{pmatrix} j^{-M} \\ \vdots \\ j^0 \\ \vdots \\ j^M \end{pmatrix} \operatorname{diag}\begin{pmatrix} J_{-M} \\ \vdots \\ J_0 \\ \vdots \\ J_M \end{pmatrix} \begin{bmatrix} e^{-jM\phi} \\ \vdots \\ e^0 \\ \vdots \\ e^{jM\phi} \end{bmatrix} + \boldsymbol{\varepsilon} \tag{47}$$

where $\operatorname{diag}(\cdot)$ is a diagonal matrix where the components along the main diagonal are the elements between the brackets. By multiplying the entire (47) from the left-hand side by $\sqrt{N}$, we can then notice that $\mathbf{V} = \sqrt{N}[\mathbf{w}_{-M} \vdots \cdots \vdots \mathbf{w}_0 \vdots \cdots \vdots \mathbf{w}_{-M}]$ so that on the left-hand side of (47), we have the term $\mathbf{V}^H\mathbf{a}(\boldsymbol{\vartheta})$. At this point, by exploiting the properties of the Bessel functions for which $J_{-m} = (-1)^m J_m$ and the relationships among the imaginary unit for which $j^{-m}(-1)^m = j^m$, we can then manipulate (47) obtaining

$$\mathbf{C}_v\mathbf{V}^H\mathbf{a}(\boldsymbol{\vartheta}) = \sqrt{N}\mathbf{J}_\zeta\mathbf{d}(\phi) + \sqrt{N}\mathbf{C}_v\boldsymbol{\varepsilon}$$

which is the same as (13).

Appendix II
Derivation of (34) and (35)

The Bessel's first integral is defined as

$$J_n(\zeta) = \frac{1}{2\pi j^n}\int_0^{2\pi} e^{j\zeta\cos(\gamma)}e^{jn\gamma}\,\mathrm{d}\gamma. \tag{48}$$

Hence, by substituting $n = m - N$ in (48), by using the modulation theorem, by exploiting some basic properties of the Bessel functions and relationships among the imaginary unit we can write

$$j^\alpha J_\alpha(\zeta)e^{-j\alpha\phi} = \frac{1}{2\pi}\int_0^{2\pi} e^{j\zeta\cos(\phi-\gamma)}e^{j(m-N)\gamma}\,\mathrm{d}\gamma \tag{49}$$

where $\alpha = N - m$. Equation (49) is the same as (34). Similarly, by substituting $n = N + m$ in (48), we could also derive (35).

APPENDIX III
NUMERICAL COMPUTATION OF (34) AND (35)

The arguments of the integrals $e^{j\zeta\cos(\phi-\gamma)}e^{j(m-N)\gamma}$ and $e^{j\zeta\cos(\phi-\gamma)}e^{j(N+m)\gamma}$ depend on the unknown DoA angle ϕ that we want to estimate and on the variable γ that describes a point on a circle. Hence a direct evaluation of (34) and (35) is not possible. This means that the integrals should be approximated by a finite sum (remember that we are working with a few sensors) [see (6) and (7)] and this may lead to creating other orders of residual terms.

However, theoretically, we may compute the integrals as a sum of finite terms only if the number of elements in the sum is high enough [2]. The solution to this problem is one of the key points of the proposed algorithm for bias cancellation. The idea is to form the argument of the integrals $e^{j\zeta\cos(\phi-\gamma)}$ in the second step of the algorithm by using the DoA estimates from the first step; see Table II. In fact, since we have constructed the argument of the integral by using the previous DoAs, we can discretize γ on a arbitrary number of points without taking into account the original UCA sensors position. In simulation studies, we see that a large enough number of points appears to be $Q = 24$. Therefore, we can rewrite (34) and (35) as

$$\frac{1}{Q}\sum_{q=0}^{Q-1} e^{j\zeta\cos(\phi-\gamma_q)}e^{j(m-N)\gamma_q} = j^{(N-m)}J_{(N-m)}(\zeta)e^{-j(N-m)\phi} + O\left(\left\|\gamma_q^2\right\|\right) \quad (50)$$

$$\frac{1}{Q}\sum_{q=0}^{Q-1} e^{j\zeta\cos(\phi-\gamma_q)}e^{j(N+m)\gamma_q} = j^{(N+m)}J_{(N+m)}(\zeta)e^{j(N+m)\phi} + O\left(\left\|\gamma_q^2\right\|\right) \quad (51)$$

where $\gamma_q = (2\pi q/Q)$ for $q = 0, \ldots, Q-1$ and $O(\|\gamma_q^2\|)$ are small terms that can be neglected without any consequences.

REFERENCES

[1] D. E. N. Davies, A. W. Rudge, Ed., *The Handbook of Antenna Design*. London, U.K.: Peregrinus, 1983, vol. 2, ch. 12.

[2] C. P. Mathews and M. D. Zoltowski, "Eigenstructure techniques for 2-D angle estimation with uniform circular arrays," *IEEE Trans. Signal Process.*, vol. 42, no. 9, pp. 2395–2407, Sep. 1994.

[3] A. J. Barabell, "Improving the resolution performance of eigenstructure-based direction-finding algorithm," in *IEEE Int. Conf. Acoust., Speech, Signal Process. (ICASSP'83)*, Apr. 1983, vol. 8, pp. 336–339.

[4] F. Belloni and V. Koivunen, "Unitary root-MUSIC technique for uniform circular array," in *Proc. 3rd Int. Symp. Signal Process. Inf. Technol. (ISSPIT)*, Darmstadt, Germany, Dec. 14–17, 2003.

[5] P. S. Naidu, *Sensor Array Signal Process*. Boca Raton, FL: CRC Press, 2001, ch. 2 and 4, pp. 75–131, 207–314.

[6] P. Stoica and A. Nehorai, "Comparative performance of element-space and beam-space MUSIC estimators," *Circuits, Syst., Signal Process.*, vol. 10, no. 3, pp. 285–291, 1991.

[7] K. M. Reddy and V. U. Reddy, "Analysis of spatial smoothing with uniform circular arrays," *IEEE Trans. Signal Process.*, vol. 47, no. 6, pp. 1726–1730, Jun. 1999.

[8] M. Wax and J. Sheinvald, "Direction finding of coherent signals via spatial smoothing for uniform circular arrays," *IEEE Trans. Antennas Propag.*, vol. 42, pp. 613–620, May 1994.

[9] D. A. Linebarger, R. D. DeGroat, and E. M. Dowling, "Efficient direction-finding methods employing forward/back averaging," *IEEE Trans. Signal Process.*, vol. 42, no. 8, pp. 2136–2145, Aug. 1994.

[10] W. Radich, R. Hamza, and K. Buckley, "Robustness and sensitivity analysis for eigenspace localization methods," in *Advances in Spectrum Analysis and Array Processing*. Englewood Cliffs, NJ: Prentice-Hall, 1995, vol. 3, ch. 3, pp. 97–111.

[11] A. L. Swindlehurst and T. Kailath, "A performance analysis of subspace-based methods in the presence of model errors—I: The MUSIC algorithm," *IEEE Trans. Signal Process.*, vol. 40, no. 7, pp. 1758–1774, Jul. 1992.

[12] M. Haardt and J. A. Nossek, "Unitary ESPRIT: How to obtain increased estimation accuracy with a reduced computational burden," *IEEE Trans. Signal Process.*, vol. 43, no. 5, pp. 1232–1242, May 1995.

[13] P. Stoica and A. Nehorai, "MUSIC, maximum likelihood, and Cramer–Rao bound," *IEEE Trans. Acoust., Speech, Signal Process.*, vol. 37, no. 5, pp. 720–741, May 1989.

[14] P. Stoica, E. G. Larsson, and A. B. Gershman, "The stochastic CRB for array processing: A textbook derivation," *IEEE Signal Process. Lett.*, vol. 8, no. 5, pp. 148–150, May 2001.

[15] B. D. Rao and K. V. S. Hari, "Performance analysis of root-MUSIC," *IEEE Trans. Acoust., Speech, Signal Process.*, vol. 37, no. 12, pp. 1939–1949, Dec. 1989.

[16] E. Grosicki, K. Abed Meraim, and W. Muhammad, "Joint angle and delay estimation using uniform circular array receiver," in *XI Eur. Signal Process. Conf. (EUSIPCO'02)*, Toulouse, France, Sep. 3–6, 2002, vol. I, pp. 81–84.

[17] P. Hyberg, M. Jansson, and B. Ottersten, "Array interpolation and bias reduction," *IEEE Trans. Signal Process.*, vol. 52, no. 10, pp. 2711–2720, Oct. 2004.

[18] L. Fu and R. J. Vaccaro, "Statistical comparison of subspace based DOA estimation algorithms in the presence of sensor errors," in *Proc. 5th ASSP Workshop Spectrum Estim. Model. 1990*, Oct. 10–12, 1990, pp. 327–331.

[19] F. Belloni, A. Richter, and V. Koivunen, "Reducing excess variance in beamspace methods for uniform circular array," in *Proc. IEEE Workshop Statist. Signal Process. (SSP)*, Bordeaux, France, Jul. 17–20, 2005.

Fabio Belloni (S'03) was born in Italy in 1978. He received the M.Sc.(Tech.) degree in telecommunication engineering from Politecnico di Milano, Milan, Italy, in 2003. He is currently pursuing the Ph.D. degree at the Helsinki University of Technology (HUT), Finland.

Since September 2002, he has been with the Signal Processing Laboratory, Department of Electrical and Communication Engineering, HUT. His research interests are in the field of multiantenna communications, channel-parameters estimation, and array signal processing.

Visa Koivunen (S'87–M'87–SM'98) received the D.Sc.(Tech.) degree (with honors) from the Department of Electrical Engineering, University of Oulu, Finland.

From 1992 to 1995, he was a Visiting Researcher at the University of Pennsylvania, Philadelphia. In 1996 he was with the Faculty of the Department of Electrical Engineering, University of Oulu. From 1997 to 1999, he was an Associate Professor with the Signal Processing Laboratory, Tampere University of Technology. Since 1999, he has been a Professor of signal processing at the Department of Electrical and Communications Engineering, Helsinki University of Technology, Finland. He is one of the Principal Investigators in the SMARAD Center of Excellence in Radio and Communications Engineering nominated by the Academy of Finland. Since 2003, he has been an Adjunct Professor at the University of Pennsylvania, Philadelphia. His research interest include statistical, communications, and sensor array signal processing. He has published more than 190 papers in international scientific conferences and journals. He is a member of the Editorial Board of *Signal Processing*.

Prof. Koivunen was an Associate Editor of IEEE SIGNAL PROCESSING LETTERS. He is a member of the IEEE Signal Processing for Communication Technical Committee.